Atomistic molecular simulations of Aβ-Zn conformational ensembles

Julen Aduriz-Arrizabalaga, Xabier López, and David De Sancho*

Polimero eta Material Aurreratuak: Fisika, Kimika eta Teknologia, Kimika Fakultatea, UPV/EHU & Donostia International Physics Center (DIPC), PK 1072, 20018 Donostia-San Sebastian, Euskadi, Spain

E-mail: david.desancho@ehu.eus

Abstract

The amyloid-forming Aβ peptide is able to interact with metal cations to form very stable complexes that influence fibril formation and contribute to the onset of Alzheimer's disease. Multiple structures of fragments of Aβ with different metals have been resolved experimentally to provide an atomic-level description of the metal-protein interactions. However, Aβ is an intrinsically disordered protein (IDP), which is more amenable to an ensemble description. Molecular dynamics (MD) simulations can now reach the timescales needed to generate ensembles for this type of complexes. However, this requires accurate force fields both for the IDP and for the protein-metal interactions. Here we use state-of-the-art methods to generate force field parameters for the Zn(II) cations in a set of Aβ complexes and combine them with the Amber99SB*-ILDN optimized force field. We show that the new parameters provide an accurate description of the molecular ensembles for IDP-metal complexes. These ensembles are more heterogeneous than the NMR models deposited in the Protein Data Bank. We validate our results against experimental data and further optimize the ensembles using a Bayesian/Maximum entropy approach.

Introduction

Alzheimer's disease is the leading cause of senile dementia and has over 55 million cases reported by the World Health Organisation as of 2021.[1] Although the cause of Alzheimer's is not completely known, a relation with aggregation and deposition of Aβ in neural tissue is widely accepted as a contributing factor to the onset of the disease. Transition metal ions and oxidative metabolism have been proposed to play fundamental roles in the process of aggregation and deposition of Aβ.[2] The binding of divalent metals, such as copper, iron, and zinc, with disordered fibrilogenic proteins, such as Aβ, influences the aggregation process of the protein, contributing directly to the severity of the neurodegenerative disease.[3] It has been reported that both the monomeric and oligomeric forms of Aβ are neurotoxic[4] and that these cations directly influence toxicity.[5] Interestingly, the Zn(II) ion concentration in the brain[6] of around 150 μM is an order of magnitude higher than the ion concentration in blood. Furthermore, even though the Zn(II) concentrations remain relatively constant through adult life, a significantly elevated concentration has been found on the brains of patients affected by Alzheimer's disease.[7] Therefore, the role Zn(II) plays in Alzheimer's disease has become of great interest.

Despite the relevance of the interactions between Aβ and transition metals to disease, their details remain elusive. This is partly due to Aβ being an intrinsically disordered protein (IDP), which makes an ensemble description preferable to the static structures derived from experimental methods such as X-ray crystallography or Nuclear Magnetic Resonance (NMR).[8] Additionally, Zn(II) characterization is highly limited by its physico-chemical properties. Out of its three stable isotopes, only ^{67}Zn is NMR active, but due to its low natural abundance and low receptivity, only solid-state, low-temperature NMR studies of zinc compounds are practically achievable. In addition, zinc complexes have no absorbance in the UV-Vis and microwave spectral regions, and its completely filled d^{10} orbitals render it diamagnetic, being, therefore, invisible in EPR spectroscopy.[9] All these factors combined make experimental studies of Aβ-Zn(II) systems highly challenging. Computer simulations are

ideally suited to complement experiments in our understanding of these types of systems.

Modelling complexes of Aβ with transition metals like Zn(II) is however not without its own challenges. First, the chemical flexibility of Zn(II) allows it to adopt different coordination modes with Aβ (see Figure 1). In the experimentally resolved structures of Aβ with Zn(II) complexes, we find the metal tetrahedrally coordinated by glutamic/aspartic acid and/or histidine residues,[10] making different combinations possible. Hence, modelers have multiple possibilities to simulate the protein-transition metal interactions.[11] The simplest option is through nonbonded models, where the metal ion interacts via electrostatic and Van der Waals interactions. Nonbonded models have successfully been used in the past.[12–15] However, in the case of Zn(II) nonbonded models often result in the wrong coordination, and the metal may even leave the coordination site.[11] This problem may be particularly acute for complexes with IDPs, where the metal may be more solvent-exposed than in globular proteins. In order to overcome these limitations, one possibility is to use "dummy models", which contain virtual atoms with point charges that promote the target coordination.[16,17] Unfortunately, they have been reported to undergo dissociation in long-time scale simulations.[11] Alternatively, one can use constraints to force the coordination of metal binding.[10,18,19] Nonetheless, it has been reported that improbable fluctuations appeared using this approach.[11] A more widely used approach consists of the use of bonded models, where chemical bonds are defined between the protein and the metal, which keep the coordination stable throughout the whole simulation time. Bonded models have been used extensively for zinc-containing systems,[2,20–22] including Aβ-metal complexes.[3,23–26]

The modeling of Aβ-Zn(II) complexes is further complicated by the disordered nature of Aβ.[8] IDPs lack a well-defined native structure and are thus best described as an ensemble of conformations. Simulating IDPs hence requires classical force fields carefully parametrized to avoid too strong structural propensities favoring folded states.[27,28] In the last few years, extensive work has dramatically improved the ability of force fields to reproduce experimental data on peptides, unfolded states of proteins and IDPs.[29,29–35] The remaining inaccuracies in

the simulated ensembles can be alleviated using integrative approaches, where experimental data is used as input in the modeling.[36] One possibility is to restrain simulations to match the experimental data available. In the case of heterogeneous systems, this approach may bias the sampling towards conformations that are not representative of any of the relevant states.[37] Alternatively, maximum-entropy approaches help generate conformational ensembles that are also compatible with the prior knowledge of the system given, in the case of biomolecular simulations, by the force field.[37,38] Specifically, Bayesian/Maximum entropy reweighting approaches optimize statistical weights of the snapshots sampled in molecular simulations in order to maximize the agreement with experimental data. These approaches have recently been used in various systems, such as RNA tetranucleotides[39] or IDP systems.[40,41]

In this work, we present conformational ensembles of Aβ-Zn(II) complexes with different coordinations and in different oligomeric states that we have parametrized using the metal center parameter builder package (MCPB.py) developed by Li and Merz.[42] This approach has recently been used to study complexes of Aβ with Zn(II),[43] Cu(II) and Al(III).[26] Here we combine the resulting parameters with the optimized Amber99SB*-ILDN force field,[44] which includes corrections for backbone[30] and sidechain torsions[31] to the ff99SB force field[45] that better capture experimental structural propensities in short peptides. In a recent study comparing multiple force fields to study Aβ_{42}, this modified force field produced results that compared extremely well against experiments.[46] We have used these parameter sets to run molecular simulations and validated them against experimental data including NMR chemical shifts and NOEs. Although we find a good agreement between simulation and experiment, we further improve the ensembles using a recently developed Bayesian/Maximum entropy reweighting method.[37] Our results indicate that Aβ-Zn(II) conformational ensembles may be more heterogeneous than suggested by the NMR models deposited in the Protein Data Bank.

Materials and methods

Aβ-Zn(II) models

In order to find minimal model systems for the study of protein-metal interactions, we queried the Protein Data Bank for entries from the full length Aβ protein in complex with Zn(II). The results of this search include structural models of peptides of different variants of human and rat Aβ either as monomers or dimers (see Table 1). Sequence lengths vary between 10 and 16 residues from the N-terminus of Aβ and include all the amino acid residues that have been proposed to interact with the Zn(II) cation.[10,47] The structures of these peptides have been resolved using solution NMR in the presence of Zn^{2+} in the form of either monomers or dimers, with one or two cations per complex. All models have different ligand combinations (see Figure 1). In all four cases, NOE restraints are available at the NMR Restraints Grid, and for all dimers chemical shifts are also available at the Biological Magnetic Resonance Database (BMRB).

Table 1: Molecular systems included in this study

PDBid	BMRB	Description	Sequence	Oligomerization	#Zn(II) cations
1ZE9[47]	-	Human Aβ WT	`Ac-DAEFRHDSGYEVHHQK-NH2`	Monomer	1
5LFY[48]	34019	Human Aβ D7H	`DAEFRHHSGY-NH2`	Dimer	2
2LI9[49]	19602	Rat Aβ	`Ac-DAEFGHDSGFEVRHQK-NH2`	Dimer	1
2MGT[50]	17884	Human Aβ H6R	`Ac-DAEFRRDSGYEVHHQK-NH2`	Dimer	1

Parametrization of protein-metal interactions

All bonded models used have been parametrized using the MCPB.py tool by Merz and co-workers,[42] which is distributed with Ambertools[1]. We performed all DFT quantum mechanical calculations using the B3LYP/6-31G*[51,52] method in the Gaussian16 package.[53] For each of the model systems, generating new parameters requires three different steps: geometry optimization, estimation of force constants using the Seminario method[54] and calculation

[1] https://ambermd.org/AmberTools.php

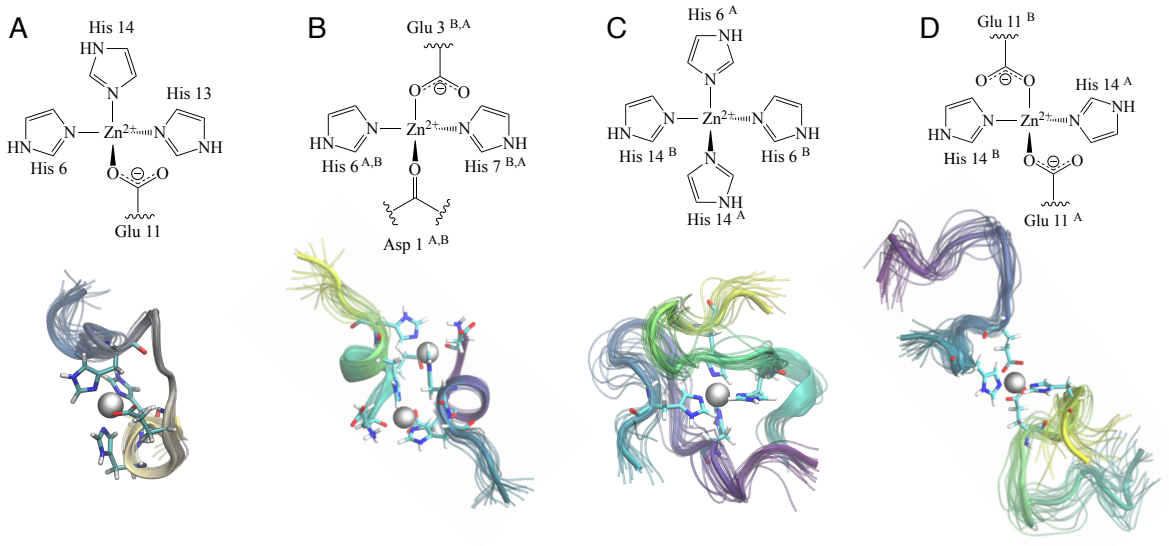

Figure 1: Cartoon representation of the metal centers (top) and cartoon representation of Aβ-Zn(II) ensembles of experimentally characterized systems (bottom). PDB ID: 1ZE9 (A), 5LFY (B), 2LI9 (C) and 2MGT (D).

of point charges using the restrained electrostatic potential (RESP) model.[55]

Three out of four of the systems we are studying are protein dimers, where two exact copies of the same protein chain are coordinated to either one or two Zn(II) cations. Due to minor discrepancies between dimers present in the experimental structures, we have obtained slightly different values of equilibrium geometry parameters, force constants, and charges for the atoms in each of the chains. To make the two chains in the dimers indistinguishable in our simulations, the protein-metal force field parameters obtained should be exactly the same. We have followed the approach taken by Peters et al. when parametrizing the ZAFF force field[21] and averaged the charges, equilibrium geometry parameters and force constants of bonds, angles and dihedrals of all duplicate values. Thereby, we have obtained the same parameter sets for both protein chains present in dimer systems.

All the files used to parametrize the bonded models and the resulting parameters are available at `https://osf.io/y4zk5/`.

Molecular dynamics simulations

We have inserted all systems within cubic boxes filled and solvated them with TIP3P water molecules.[56] We added a 0.1 M concentration of Cl^- and Na^+ ions to all systems, and also neutralized the total charge of the system when necessary. The systems were energy-minimized using the steepest descent algorithm and then equilibrated in two stages. First, we run a 100 ps simulation in the NVT ensemble and then another 100 ps in the NPT ensemble, both including position restraints in the protein heavy atoms. Molecular Dynamics (MD) simulations were performed in the NVT ensemble, using an integration time step of 2 fs. Constant temperature and pressure were set by coupling the system to a Parrinello-Rahman barostat at 1.0 bar and a velocity-rescaling thermostat at 278 K,[57–59] corresponding to the temperature of the NMR experiments. Equilibrium simulations were run for 5 μs with the Amber99SB*-ILDN force field[30,31] using the Gromacs software package (version 2020).[60]

Analysis, validation, and reweighting

To analyze the results of the simulations we have used a combination of Gromacs tools and in-house scripts using the MDtraj Python library.[61] We have validated the results of our simulations against experiments back-calculating a series of NMR observables from the simulations. We used the SPARTA+ program to back-calculate chemical shifts.[62] Additionally, we estimate distances corresponding to the observed NOEs using r^{-6} averaging.[63–65]

We additionally perform a Bayesian/Maximum entropy reweighting using the BME program[37] to refine simulations using the experimental data available, in this case NOE distance restraints. The main goal of the reweighting of simulations is to obtain an optimized set of statistical weights for the simulation ensemble that are in better agreement with experiments given a forward model for the experimental observable.[36] More information about BME is provided in the Supporting Information.

Results and discussion

Molecular simulations with new force fields parameters

We have used the MCBP.py package to generate parameters for bonded models for all the Aβ-Zn(II) complexes in Table 1 (see Methods). Using the new parameters, we have run 5 μs atomistic MD simulations for all four systems. In Figure 2 we show the values of the $C^{\alpha} - RMSD$ and the radius of gyration (R_g) for each of them. The $RMSD$ values typically remain under 5 Å for most of the simulation time. However, with the exception of the D7H mutant dimer (5LFY), we observe relatively large fluctuations that suggest that the simulations explore a variety of conformations that are dissimilar from those reported in the PDB. On the other hand, we find that the R_g values remain stable throughout the simulations, although two of the systems are notably more compact than the PDB models. This effect is likely due to the influence of the TIP3P water model used in our simulations, which is known to produce these effects.[66]

In order to identify the regions of the protein with the largest fluctuations, we also report values for the $RMSF$ for all systems (see Figure 3A). As expected, the highest $RMSF$ values correspond to regions at the N and C-termini of each system, except in the case of the D7H mutant dimer (5LFY). In this case, the low $RMSF$ values in the N-termini are related to the coordination of the Zn^{2+} cation by the oxygen from the carbonyl of the first amino acid in the peptide sequence. On the contrary, in the case of the monomer (1ZE9), H6R mutant dimer (2MGT) and rat Aβ dimer (2LI9), fluctuations are on average larger and their values are greatest at the N and C-termini.

The trends observed in the $RMSF$ are consistent with the very different structural propensities in the metal-bound peptides. In Figure 3B we show the assignments to different types of secondary structure obtained using the DSSP algorithm.[67] The regions that more stably keep the secondary structure coincide with those with the lowest $RMSF$ values, which also contain the chelated residues. This behavior is clearest for the D7H mutant dimer

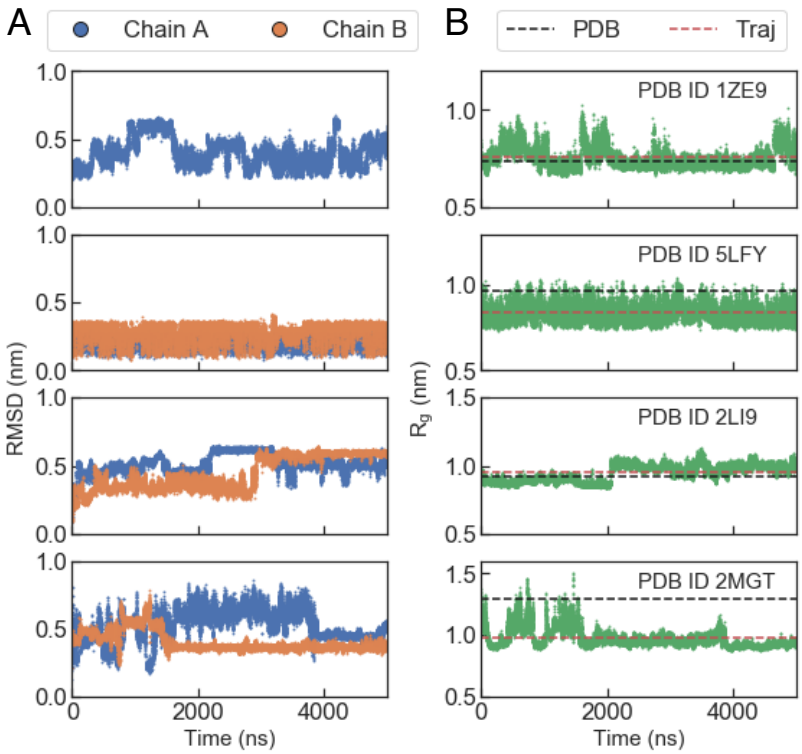

Figure 2: $RMSD$ (A) and R_g (B) values calculated from the 5 μs simulations using the parametrized bonded models. Mean R_g values calculated from PDB models are shown by black lines and mean R_g values calculated from our simulations are shown by red lines.

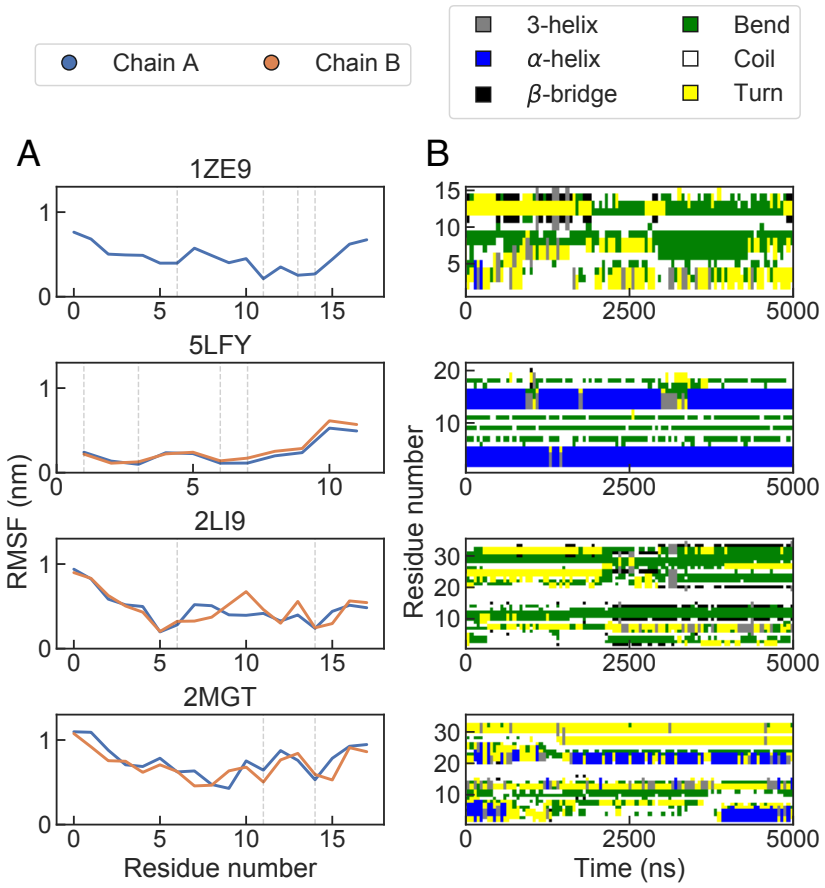

Figure 3: (A) Per-residue $RMSF$ values calculated for each of the Aβ-Zn systems. For dimers, we represent each chain with a different colour. Vertical dashed lines mark the Zn-chelating residues. (B) Secondary structure assignment calculated with DSSP.

(5LFY), where the α-helices remain fully formed in both peptide chains through almost the complete duration of the simulation trajectory.

In order to visualize the differences between the ensemble of conformations sampled during the simulations and the NMR structures, we have calculated the contact maps, which we compare with the averages from the 20 structural models deposited in the PDB for each of our systems (see Figure 4). We find that despite the intermediate values of the $RMSD$ reported above, the contact maps from the simulations are largely consistent with those of the experimental models. Specifically, close contacts from the NMR ensembles are mostly recapitulated by the simulation results. This is expected because the conformational dynamics in our complexes are restricted by the interactions with the metal cations.

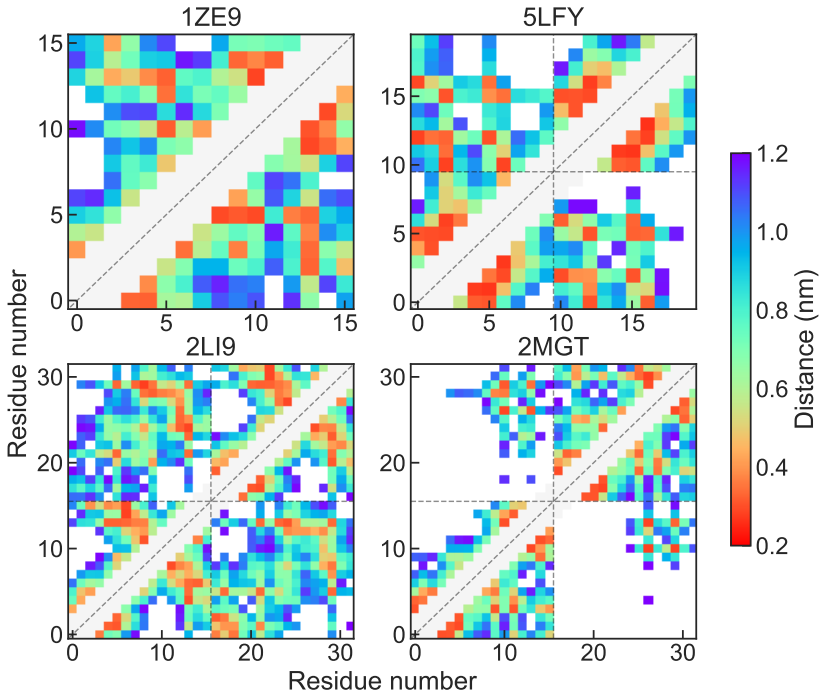

Figure 4: Contact maps calculated from PDB structures (lower diagonal) and trajectories (upper diagonal).

Validation against NMR data

In order to assess the validity of our simulations more carefully, we compare the results obtained with the combination of the new metal parameters with the Amber99SB*-ILDN force field directly against available experimental NMR data. First, we compare experimental chemical shifts with values back-calculated from the simulations using SPARTA+[62] (see Methods). In Table 2 we report the $RMSD$ and χ^2 values of the calculated chemical shifts, and compare them with those for the NMR models. Overall, both the $RMSD$ and χ^2 values obtained from the 20 structures deposited in the PDB and our 5 μs simulations are in the same range, indicating that our simulations have reached the same level of accuracy as the experimental models for the Aβ-Zn(II) systems.

There are, however, some noteworthy inconsistencies between the calculated chemical shifts and the experimental measurements (see Figure 5). For example, the simulations do not completely track the overall tendency of the chemical shift of Hα for residues 1 and 3 of the D7H mutant (5LFY model). In the case of C^{α} and C^{β} chemical shifts, the agreement is worst for the rat peptide (2LI9), although the overall trends are captured correctly. Instead, for both the D7H and H6R mutants (5LFY and 2MGT, respectively) the agreement with experiments is excellent for the carbon chemical shifts. Lastly, for the HN protons, the simulations for the rat peptide (2LI9) result in the best agreement obtained shown both from $RMSD$ and χ^2 values.

Additionally, we have calculated average distances from the simulations for all the atom pairs involved in measurable NOEs (see Figure 6). We note that for all the dimers, the intra-chain NOE distance restraint values are duplicated for chains A and B in the BMRB entries (see Figure S1). To estimate the average distances from the simulations, we assume that the chains are indistinguishable, as they are in the experiment, and keep only one set of NOE values. Accordingly, we report a single set of distances averaging distances from both chains. When no errors were reported, we arbitrarily assign a 20% to the measured value.

Overall, the simulations with the new bonded parameters and the Amber99SB*-ILDN

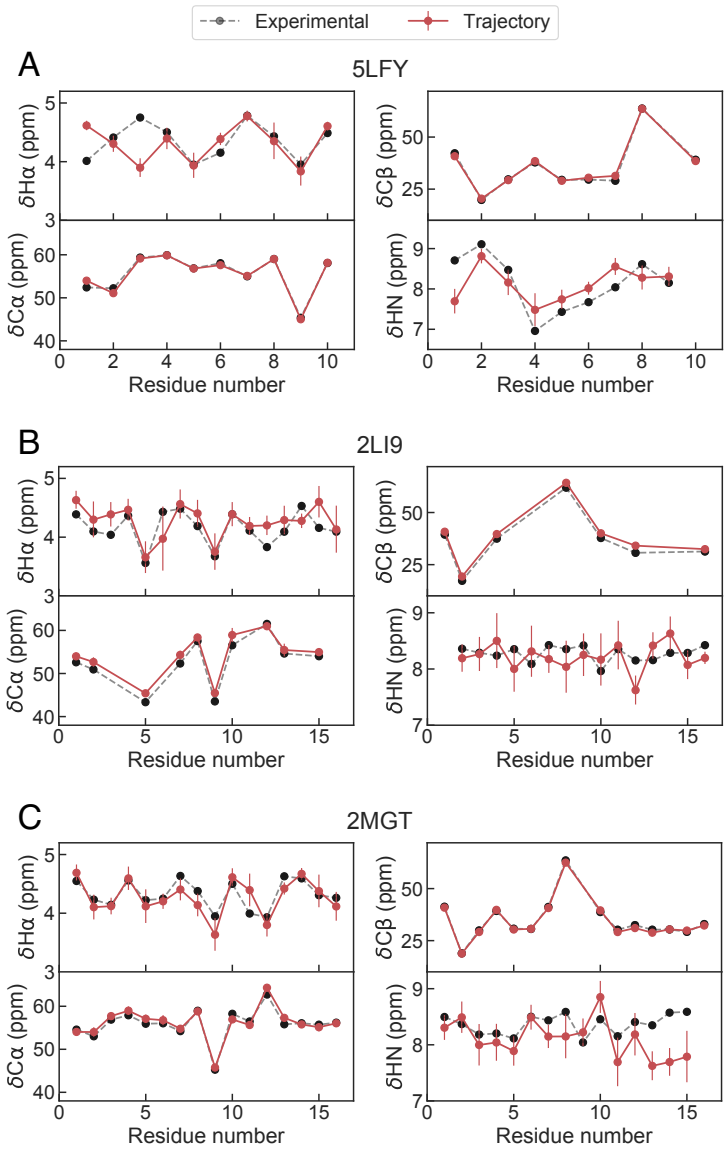

Figure 5: Chemical shifts calculated for the 5LFY (A), 2LI9 (B) and 2MGT (C) systems with experimental data available. Experimental values are shown in black and back calculated chemical shifts are shown in red.

Table 2: Calculated $RMSD$ and χ^2 values of chemical shifts back-calculated from PDB structures and 5 μs simulations.

	5LFY		2LI9		2MGT	
$RMSD$ (ppm)	PDB	Simulation	PDB	Simulation	PDB	Simulation
H^{α}	0.21	0.35	0.24	0.24	0.27	0.18
C^{α}	0.88	0.65	1.44	1.59	1.23	0.91
C^{β}	1.02	1.03	1.53	2.21	1.05	0.79
H_N	0.53	0.48	0.55	0.27	0.46	0.43
χ^2	PDB	Simulation	PDB	Simulation	PDB	Simulation
H^{α}	0.90	2.43	1.45	2.12	1.39	1.20
C^{α}	0.95	0.86	3.01	3.94	2.04	1.60
C^{β}	0.88	1.05	2.00	4.56	1.03	0.98
H_N	1.32	1.28	1.62	0.82	1.01	1.20

force field successfully capture the vast majority of the experimental NOE distances. Interestingly the χ^2 value obtained for each system is 0.078 for the monomer (1ZE9), 0.076 for the D7H mutant (5LFY), 0.088 for the H6R mutant (2MGT) and 0.081 for the rat dimer (2LI9). Nonetheless, some values of NOE distances are overestimated from the simulations e.g. distances 65 and 66 of the monomer (1ZE9), distances 0 to 10 in the rat dimer (2LI9) or distances from 15 to 20 of the H6R mutant (2MGT) (see Figure 6).

BME reweighting improves agreement with NMR data

The overestimation of some NOE distances from the unbiased simulations suggests there is room for improvement in the conformational ensembles. Therefore, we have reweighted our simulations to further improve the quality of the ensembles obtained for the systems using the BME program developed by Bottaro et al.[37] which relies on Bayesian/Maximum entropy approach (see Methods) using the NOE data from Figure 6. Ensemble reweighting helps improve the agreement with experiment for all systems, significantly in some cases, as indicated by a decrease in χ^2. After optimization the χ^2 values are of 0.050 for the monomer (1ZE9), 0.045 for the D7H mutant (5LFY), 0.045 for the rat dimer (2LI9) and 0.032 for the H6R (2MGT), a 36%, 55%, 50% and 63% improvement, respectively.

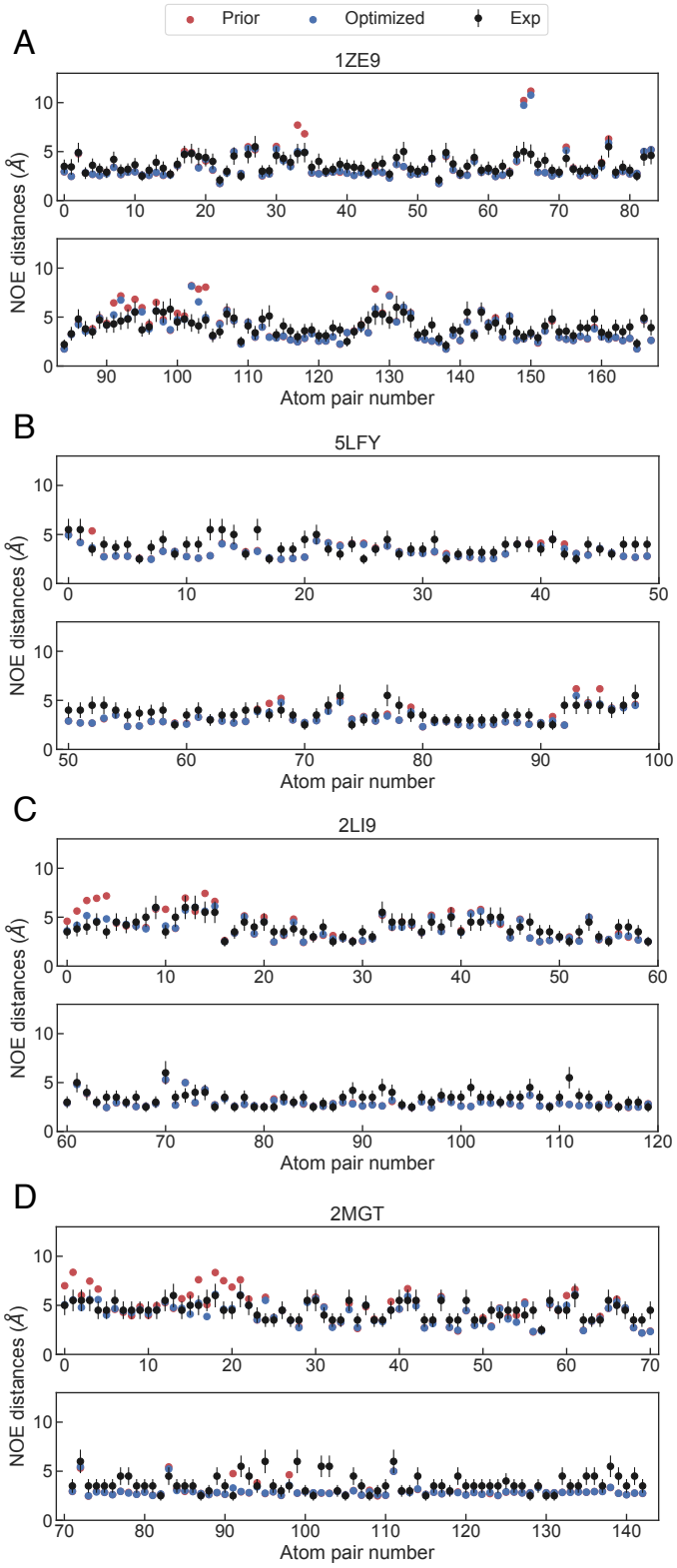

Figure 6: NOEs calculated for the the 1ZE9(A), 5LFY (B), 2LI9 (C) and 2MGT (D) systems with experimental data available. Experimental values are shown in black, back-calculated NOEs are shown in red and NOEs calculated after optimization are shown in blue.

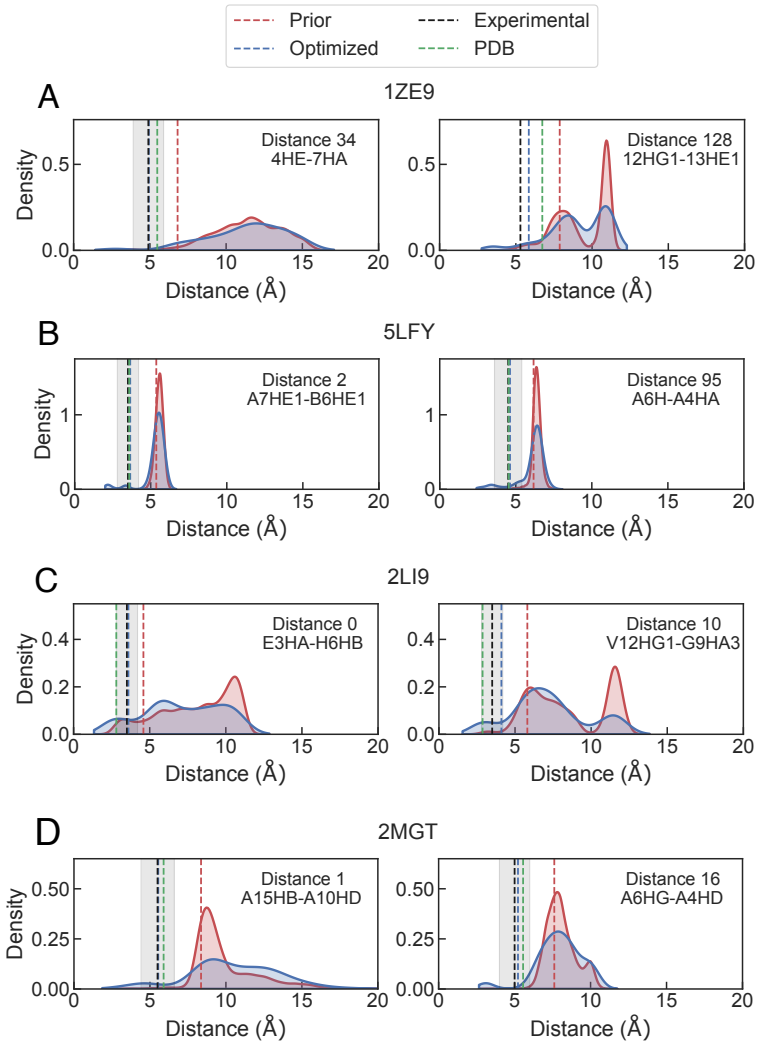

Figure 7: Distribution of distance density of two optimized NOE distances for systems 1ZE9 (A), 5LFY (B), 2LI9 (C) and 2MGT (D). Experimental values are shown in black, experimental uncertainty is shown in grey, values extracted from simulations are shown in red, and reweighted values are shown in blue. The values calculated from the PDB structures are shown in green.

In order to understand the effect of the reweighting, we have inspected the distribution of distances before and after optimization (see Figure 7). We illustrate the improvement for few pairs whose average distances did not originally match the experimental value in our unbiased simulations. Due to the exponential averaging of distances, a gentle shift in the distribution results in a considerable improvement in the agreement, except for D7H mutant where improvement is modest (see Figure S5). Remarkably, even after optimization, long distance conformations remain present in the distribution, resulting in average values that are as compatible with the experiment as those from the 20 NMR models (see e.g. E3HA-H6HB form 2LI9).

Conclusions

In this work, we have produced bonded Zn(II) models of four Aβ-Zn(II) systems for the Amber99SB*-ILDN force field. We note that other force field-water model combinations may further improve the accuracy of the results. Using these parameters, we have run 5 μs simulations of four different systems and validated the results against experiments. The simulations have sampled well beyond the conformational space of the models reported in the PDB as shown by the $RMSD$ of C$^{\alpha}$ and contact maps. This extended sampling nevertheless compares well with experimentally measured chemical shifts and NOEs.

In order to improve the agreement between simulations and experiments, we have reweighted our simulations using the BME program[37] using NOE data. Interestingly, the improvement of the simulations shows that the best agreement is obtained when both collapsed and extended conformations of the systems are present in the conformational ensembles. This may have implications for our understanding of the role of Zn(II) in the aggregation of Aβ, which has been explored in the past using the more structured NMR models as initial structures for MD simulations.[10]

We hope that the parameters we have produced for all four systems will help on gaining

a better understanding of Aβ-Zn(II) interactions. The parameters that we make publicly available for all four complexes will afford more accurate simulations and may be applied in studies of primary and secondary nucleation of fibrils.[68]

Acknowledgement

Financial support comes from Eusko Jaurlaritza (Basque Government) through the project IT1584-22 and from the Spanish Ministry of Science and Universities through the Office of Science Research (MINECO/FEDER) through grant PGC2018-099321-B-I00 . DDS acknowledges the Spanish Ministry of Science and Universities for a Ramón y Cajal contract (Grant RYC-2016-19590). The authors thank Sandro Bottaro for help using the BME program and Kresten Lindorff Larsen for useful discussions. The authors also acknowledge the staff at the DIPC Supercomputing Center for technical support.

Supporting Information Available

Supplementary Methods and eight additional figures.

References

(1) Dementia. `https://www.who.int/news-room/fact-sheets/detail/dementia`, Accessed: 2023-02-14.

(2) Barnham, K. J.; Bush, A. I. Metals in Alzheimer's and Parkinson's Diseases. *Curr. Opin. Chem. Biol.* **2008**, *12*, 222–228.

(3) Wise-Scira, O.; Xu, L.; Perry, G.; Coskuner, O. Structures and Free Energy Landscapes of Aqueous Zinc (II)-Bound Amyloid-β (1–40) and Zinc (II)-Bound Amyloid-β (1–42) with Dynamics. *J. Biol. Inorg. Chem.* **2012**, *17*, 927–938.

(4) Hardy, J.; Selkoe, D. J. The Amyloid Hypothesis of Alzheimer's Disease: Progress and Problems on the Road to Therapeutics. *Science* **2002**, *297*, 353–356.

(5) Chen, T.; Wang, X.; He, Y.; Zhang, C.; Wu, Z.; Liao, K.; Wang, J.; Guo, Z. Effects of Cyclen and Cyclam on Zinc (II)-and Copper (II)-Induced Amyloid β-Peptide Aggregation and Neurotoxicity. *Inorg. Chem.* **2009**, *48*, 5801–5809.

(6) Sensi, S. L.; Paoletti, P.; Bush, A. I.; Sekler, I. Zinc in the Physiology and Pathology of the CNS. *Nat. Rev. Neurosci.* **2009**, *10*, 780–791.

(7) Deibel, M.; Ehmann, W.; Markesbery, W. Copper, Iron, and Zinc Imbalances in Severely Degenerated Brain Regions in Alzheimer's Disease: Possible Relation to Oxidative Stress. *J. Neurol. Sci.* **1996**, *143*, 137–142.

(8) Das, P.; Matysiak, S.; Mittal, J. Looking at the Disordered Proteins through the Computational Microscope. *ACS Cent. Sci.* **2018**, *4*, 534–542.

(9) Laitaoja, M.; Valjakka, J.; Janis, J. Zinc coordination spheres in protein structures. *Inorg. Chem.* **2013**, *52*, 10983–10991.

(10) Miller, Y.; Ma, B.; Nussinov, R. Zinc Ions Promote Alzheimer Aβ Aggregation via Population Shift of Polymorphic States. *Proc. Natl. Acad. Sci. U.S.A.* **2010**, *107*, 9490–9495.

(11) Strodel, B.; Coskuner-Weber, O. Transition Metal Ion Interactions with Disordered Amyloid-β Peptides in the Pathogenesis of Alzheimer's Disease: Insights from Computational Chemistry Studies. *J. Chem. Inf. Model.* **2019**, *59*, 1782–1805.

(12) Hoops, S. C.; Anderson, K. W.; Merz Jr, K. M. Force Field Design for ;etalloproteins. *J. Am. Chem. Soc.* **1991**, *113*, 8262–8270.

(13) Stote, R. H.; Karplus, M. Zinc Binding in Proteins and Solution: a Simple But Accurate Nonbonded Representation. *Proteins* **1995**, *23*, 12–31.

(14) Bredenberg, J.; Nilsson, L. Modeling Zinc Sulfhydryl Bonds in Zinc Fingers. *Int. J. Quantum Chem.* **2001**, *83*, 230–244.

(15) Yang, B.; Zhu, Y.; Wang, Y.; Chen, G. Interaction Identification of Zif268 and TATAZF Proteins with GC-/AT-rich DNA Sequence: a Theoretical Study. *J. Comput. Chem.* **2011**, *32*, 416–428.

(16) Duarte, F.; Bauer, P.; Barrozo, A.; Amrein, B. A.; Purg, M.; Åqvist, J.; Kamerlin, S. C. L. Force Field Independent Metal Parameters Using a Nonbonded Dummy Model. *J. Phys. Chem. B* **2014**, *118*, 4351–4362.

(17) Liao, Q.; Pabis, A.; Strodel, B.; Kamerlin, S. C. L. Extending the Nonbonded Cationic Dummy Model to Account for Ion-Induced Dipole Interactions. *J. Phys. Chem. Lett.* **2017**, *8*, 5408–5414.

(18) Man, V. H.; Nguyen, P. H.; Derreumaux, P. High-Resolution Structures of the Amyloid-β 1–42 Dimers from the Comparison of Four Atomistic Force Fields. *J. Phys. Chem. B* **2017**, *121*, 5977–5987.

(19) Li, W.; Zhang, J.; Wang, J.; Wang, W. Metal-Coupled Folding of Cys2His2 Zinc-Finger. *J. Am. Chem. Soc.* **2008**, *130*, 892–900.

(20) Lin, F.; Wang, R. Systematic Derivation of AMBER Force Field Parameters Applicable to Zinc-Containing Systems. *J. Chem. Theory Comput.* **2010**, *6*, 1852–1870.

(21) Peters, M. B.; Yang, Y.; Wang, B.; Fusti-Molnar, L.; Weaver, M. N.; Merz Jr, K. M. Structural Survey of Zinc-Containing Proteins and Development of the Zinc AMBER Force Field (ZAFF). *J. Chem. Theory Comput.* **2010**, *6*, 2935–2947.

(22) Yu, Z.; Li, P.; Merz Jr, K. M. Extended Zinc AMBER Force Field (EZAFF). *J. Chem. Theory Comput.* **2018**, *14*, 242–254.

(23) Pan, L.; Patterson, J. C. Molecular Dynamics Study of Zn (Aβ) and Zn (Aβ) 2. *PLoS One* **2013**, *8*, e70681.

(24) Xu, L.; Wang, X.; Wang, X. Effects of Zn2+ Binding on the Structural and Dynamic Properties of Amyloid B Peptide Associated with Alzheimer's Disease: Asp1 or Glu11? *ACS Chem. Neurosci.* **2013**, *4*, 1458–1468.

(25) Boopathi, S.; Dinh Quoc Huy, P.; Gonzalez, W.; Theodorakis, P. E.; Li, M. S. Zinc Binding Promotes Greater Hydrophobicity in Alzheimer's Aβ42 Peptide than Copper Binding: Molecular Dynamics and Solvation Thermodynamics Studies. *Proteins* **2020**, *88*, 1285–1302.

(26) Roldán-Martín, L.; Peccati, F.; Sciortino, G.; Sodupe, M.; Maréchal, J.-D. Impact of Cu (ii) and Al (iii) on the Conformational Landscape of Amyloidβ 1-42. *Phys. Chem. Chem. Phys.* **2021**, *23*, 13023–13032.

(27) Huang, J.; MacKerell Jr, A. D. Force Field Development and Simulations of Intrinsically Disordered Proteins. *Curr. Opin. Struct. Biol.* **2018**, *48*, 40–48.

(28) Shea, J.-E.; Best, R. B.; Mittal, J. Physics-Based Computational and Theoretical Approaches to Intrinsically Disordered Proteins. *Curr. Opin. Struct. Biol.* **2021**, *67*, 219–225.

(29) Best, R. B.; Buchete, N.-V.; Hummer, G. Are Current Molecular Dynamics Force Fields too Helical? *Biophys. J.* **2008**, *95*, L07–L09.

(30) Best, R. B.; Hummer, G. Optimized Molecular Dynamics Force Fields Applied to the Helix-Coil Transition of Polypeptides. *J. Phys. Chem. B* **2009**, *113*, 9004–9015.

(31) Lindorff-Larsen, K.; Piana, S.; Palmo, K.; Maragakis, P.; Klepeis, J. L.; Dror, R. O.; Shaw, D. E. Improved Side-chain Torsion Potentials for the Amber ff99SB Protein Force Field. *Proteins: Structure, Function, and Bioinformatics* **2010**, *78*, 1950–1958.

(32) Lindorff-Larsen, K.; Maragakis, P.; Piana, S.; Eastwood, M. P.; Dror, R. O.; Shaw, D. E. Systematic Validation of Protein Force Fields Against Experimental Data. *PloS one* **2012**, *7*, e32131.

(33) Huang, J.; Rauscher, S.; Nawrocki, G.; Ran, T.; Feig, M.; De Groot, B. L.; Grubmüller, H.; MacKerell Jr, A. D. CHARMM36m: an Improved Force Field for Folded and Intrinsically Disordered Proteins. *Nat. Methods* **2017**, *14*, 71–73.

(34) Robustelli, P.; Piana, S.; Shaw, D. E. Developing a Molecular Dynamics Force Field for Both Folded and Disordered Protein States. *Proc. Natl. Acad. Sci. U.S.A.* **2018**, *115*, E4758–E4766.

(35) Zerze, G. H.; Zheng, W.; Best, R. B.; Mittal, J. Evolution of All-Atom Protein Force Fields to Improve Local and Global Properties. *J. Phys. Chem. Lett.* **2019**, *10*, 2227–2234.

(36) Bottaro, S.; Lindorff-Larsen, K. Biophysical Experiments and Biomolecular Simulations: A Perfect Match? *Science* **2018**, *361*, 355–360.

(37) Bottaro, S.; Bengtsen, T.; Lindorff-Larsen, K. Integrating Molecular Simulation and Experimental Data: a Bayesian/Maximum Entropy Reweighting Approach. *Structural bioinformatics: methods and protocols* **2020**, 219–240.

(38) Hummer, G.; Köfinger, J. Bayesian Ensemble Refinement by Replica Simulations and Reweighting. *J. Chem. Phys.* **2015**, *143*, 12B634_1.

(39) Bottaro, S.; Bussi, G.; Kennedy, S. D.; Turner, D. H.; Lindorff-Larsen, K. Conformational Ensembles of RNA Oligonucleotides From Integrating NMR and Molecular Simulations. *Sci. Adv.* **2018**, *4*, eaar8521.

(40) Crehuet, R.; Buigues, P. J.; Salvatella, X.; Lindorff-Larsen, K. Bayesian-Maximum-

Entropy Reweighting of IDP Ensembles Based on NMR Chemical Shifts. *Entropy* **2019**, *21*, 898.

(41) Mantsyzov, A. B.; Maltsev, A. S.; Ying, J.; Shen, Y.; Hummer, G.; Bax, A. A Maximum Entropy Approach to the Study of Residue-Specific Backbone Angle Distributions in α-Synuclein, an Intrinsically Disordered Protein. *Protein Sci.* **2014**, *23*, 1275–1290.

(42) Li, P.; Merz Jr, K. M. MCPB. py: a Python Based Metal Center Parameter Builder. *J. Chem. Inf. Model* **2016**, *56*, 599–604.

(43) Al-Shammari, N.; Savva, L.; Kennedy-Britten, O.; Platts, J. A. Forcefield Evaluation and Accelerated Molecular Dynamics Simulation of Zn (II) Binding to N-Terminus of Amyloid-β. *Comput. Biol. Chem.* **2021**, *93*, 107540.

(44) Piana, S.; Lindorff-Larsen, K.; Shaw, D. E. How robust are protein folding simulations with respect to force field parameterization? *Biophys. J.* **2011**, *100*, L47–L49.

(45) Hornak, V.; Abel, R.; Okur, A.; Strockbine, B.; Roitberg, A.; Simmerling, C. Comparison of Multiple Amber Force Fields and Development of Improved Protein Backbone Parameters. *Proteins* **2006**, *65*, 712–725.

(46) Carballo-Pacheco, M.; Strodel, B. Comparison of force fields for Alzheimer's A: A case study for intrinsically disordered proteins. *Protein Sci.* **2017**, *26*, 174–185.

(47) Zirah, S.; Kozin, S. A.; Mazur, A. K.; Blond, A.; Cheminant, M.; Ségalas-Milazzo, I.; Debey, P.; Rebuffat, S. Structural Changes of Region 1-16 of the Alzheimer Disease Amyloid β-Peptide Upon Zinc Binding and in vitro Aging. *J. Biol. Chem.* **2006**, *281*, 2151–2161.

(48) Polshakov, V. I.; Mantsyzov, A. B.; Kozin, S. A.; Adzhubei, A. A.; Zhokhov, S. S.; van Beek, W.; Kulikova, A. A.; Indeykina, M. I.; Mitkevich, V. A.; Makarov, A. A. A

Binuclear Zinc Interaction Fold Discovered in the Homodimer of Alzheimer's Amyloid-β Fragment with Taiwanese Mutation D7H. *Angew. Chem.* **2017**, *129*, 11896–11901.

(49) Istrate, A. N.; Tsvetkov, P. O.; Mantsyzov, A. B.; Kulikova, A. A.; Kozin, S. A.; Makarov, A. A.; Polshakov, V. I. NMR Solution Structure of Rat Aβ (1–16): Toward Understanding the Mechanism of Rats' Resistance to Alzheimer's Disease. *Biophys. J.* **2012**, *102*, 136–143.

(50) Istrate, A. N.; Kozin, S. A.; Zhokhov, S. S.; Mantsyzov, A. B.; Kechko, O. I.; Pastore, A.; Makarov, A. A.; Polshakov, V. I. Interplay of Histidine Residues of the Alzheimer's Disease Aβ Peptide Governs its Zn-Induced Oligomerization. *Sci. Rep.* **2016**, *6*, 1–14.

(51) Stephens, P. J.; Devlin, F. J.; Chabalowski, C. F.; Frisch, M. J. Ab initio Calculation of Vibrational Absorption and Circular Dichroism Spectra Using Density Functional Force Fields. *J. Phys. Chem. A* **1994**, *98*, 11623–11627.

(52) Hehre, W. J.; Ditchfield, R.; Pople, J. A. Self—Consistent Molecular Orbital Methods. XII. Further Extensions of Gaussian—Type Basis Sets for Use in Molecular Orbital Studies of Organic Molecules. *Chem. Phys.* **1972**, *56*, 2257–2261.

(53) Frisch, M. J. et al. Gaussian˜16 Revision C.01. 2016; Gaussian Inc. Wallingford CT.

(54) Seminario, J. M. Calculation of Intramolecular Force Fields from Second-Derivative Tensors. *Int. J. Quantum Chem.* **1996**, *60*, 1271–1277.

(55) Bayly, C. I.; Cieplak, P.; Cornell, W.; Kollman, P. A. A well-behaved Electrostatic Potential Based Method Using Charge Restraints for Deriving Atomic Charges: the RESP Model. *J. Phys. Chem.* **1993**, *97*, 10269–10280.

(56) Jorgensen, W. L.; Chandrasekhar, J.; Madura, J. D.; Impey, R. W.; Klein, M. L.

Comparison of Simple Potential Functions for Simulating Liquid Water. *Chem. Phys.* **1983**, *79*, 926–935.

(57) Bussi, G.; Donadio, D.; Parrinello, M. Canonical Sampling Through Velocity Rescaling. *J. Chem. Phys.* **2007**, *126*, 014101.

(58) Parrinello, M.; Rahman, A. Polymorphic Transitions in Single Crystals: A new Molecular Dynamics Method. *J. Appl. Phys.* **1981**, *52*, 7182–7190.

(59) Nosé, S.; Klein, M. Constant Pressure Molecular Dynamics for Molecular Systems. *Mol. Phys.* **1983**, *50*, 1055–1076.

(60) Abraham, M. J.; Murtola, T.; Schulz, R.; Páll, S.; Smith, J. C.; Hess, B.; Lindahl, E. GROMACS: High Performance Molecular Simulations Through Multi-Level Parallelism from Laptops to Supercomputers. *SoftwareX* **2015**, *1-2*, 19–25.

(61) McGibbon, R. T.; Beauchamp, K. A.; Harrigan, M. P.; Klein, C.; Swails, J. M.; Hernández, C. X.; Schwantes, C. R.; Wang, L.-P.; Lane, T. J.; Pande, V. S. MDTraj: A Modern Open Library for the Analysis of Molecular Dynamics Trajectories. *Biophys. J.* **2015**, *109*, 1528 – 1532.

(62) Shen, Y.; Bax, A. SPARTA+: a Modest Improvement in Empirical NMR Chemical Shift Prediction by Means of an Artificial Neural Network. *J. Biol. NMR* **2010**, *48*, 13–22.

(63) Tropp, J. Dipolar Relaxation and Nuclear Overhauser Effects in Nonrigid Molecules: the Effect of Fluctuating Internuclear Distances. *J. Chem. Phys.* **1980**, *72*, 6035–6043.

(64) Rieping, W.; Habeck, M.; Nilges, M. Inferential Structure Determination. *Science* **2005**, *309*, 303–306.

(65) Daura, X.; Antes, I.; van Gunsteren, W. F.; Thiel, W.; Mark, A. E. The Effect of

Motional Averaging on the Calculation of NMR-Derived Structural Properties. *Proteins* **1999**, *36*, 542–555.

(66) Shabane, P. S.; Izadi, S.; Onufriev, A. V. General Purpose Water Model Can Improve Atomistic Simulations of Intrinsically Disordered Proteins. *J. Chem. Theory Comput.* **2019**, *15*, 2620–2634.

(67) Kabsch, W.; Sander, C. Dictionary of Protein Secondary Structure: Pattern Recognition of Hydrogen-Bonded and Geometrical Features. *Biopolymers* **1983**, *22*, 2577–2637.

(68) Bellaiche, M. M.; Best, R. B. Molecular Determinants of Aβ42 Adsorption to Amyloid Fibril Surfaces. *J. Phys. Chem. Lett* **2018**, *9*, 6437–6443.